Ultramicroscopy 108 (2008) 1401–1407

Contents lists available at ScienceDirect

Ultramicroscopy

journal homepage: www.elsevier.com/locate/ultramic

Quantitative electron holographic tomography for the 3D characterisation of semiconductor device structures

Alison C. Twitchett-Harrison *, Timothy J.V. Yates, Rafal E. Dunin-Borkowski [1], Paul A. Midgley

Department of Materials Science and Metallurgy, University of Cambridge, Pembroke Street, Cambridge, CB2 3QZ, UK

ARTICLE INFO

PACS:
81.05Cy
68.37Lp
85.30De
61.05jp

Keywords:
Electron holography
Electron tomography
Silicon devices
Device characterisation

ABSTRACT

Electron tomography and electron holography experiments have been combined to investigate the 3D electrostatic potential distribution in semiconductor devices. The experimental procedure for the acquisition and data reconstruction of holographic tilt series of silicon p–n junction specimens is described. A quantitative analysis of the experimental results from specimens of two different thicknesses is presented, revealing the 3D electrostatic potential variations arising from the presence of surfaces and damage generated by focused ion beam (FIB) sample preparation. Close to bulk-like properties are measured in the centre of the tomographic reconstruction of the specimen, revealing higher electrically active dopant concentrations compared to the measurements obtained at the specimen surfaces. A comparison of the experimental results from the different thickness specimens has revealed a 'critical' thickness for this specimen preparation method of 350 nm that is required for this device structure to retain 'bulk'-like properties in the centre of the membrane.

1. Introduction

Dopant profiling of semiconductor devices using off-axis electron holography has become more widely used in recent years, with many examples of the successful visualisation of dopant-related electrostatic potentials [1,2]. Although many other techniques are available for the determination of electrostatic potential distributions [3], only off-axis electron holography can provide directly quantifiable results with nanometre-scale spatial resolution. Off-axis electron holography is a transmission electron microscope (TEM)-based interference technique that allows the phase shift of an electron wave to be quantified, thus allowing the electrostatic potential distribution to be determined. This technique has been highlighted as a potential solution for the 2D mapping of potential distributions in semiconductor device structures [4], and promises to provide high spatial resolution 2D maps of the dopant-related potential.

With the miniaturisation of device structures, it is increasingly important to be able to resolve the electrostatic device properties in three dimensions, information which can be obtained through the use of combined electron holography and electron tomography [5]. Electron tomography uses a series of images acquired over a high range of specimen tilt angles to reconstruct 3D information about a sample, and has previously been applied successfully to the examination of small particles such as catalysts [6]. However, for the application of electron tomography to the reconstruction of 3D electrostatic potentials many additional issues must be considered because the potentials are continuous, extended functions, unlike the isosurfaces conventionally reconstructed using electron tomography. The boundary conditions including surface potentials and specimen thickness must, therefore, be carefully considered, and will be discussed in more detail later in this paper.

One important criterion that must be satisfied for successful electron tomography is the 'projection requirement' [7], which states that the signal of interest must be a monotonic function of the specimen thickness. The phase shift ($\Delta\varphi$) measured using electron holography for a thin specimen containing only electrostatic potentials (i.e. no magnetic potentials) is given by Eq. (1).

$$\Delta\varphi = C_E \int V(x,y,z)\,dz \tag{1}$$

where $V(x,y,z)$ is the electrostatic potential distribution, z is the electron beam direction and C_E is a microscope determined constant. If the specimen is carefully positioned to avoid strongly diffracting conditions, the electrostatic potential contribution $V(x,y,z)$ can be defined as

$$V(x,y,z) = V_0(x,y,z) + V_d(x,y,z) \tag{2}$$

where $V_0(x,y,z)$ is the mean inner potential of the specimen, and $V_d(x,y,z)$ is the dopant-related variation in electrostatic potential.

* Corresponding author at: Imperial College London and London Centre for Nanotechnology, Exhibition Road, London. SW7 2AZ, UK.
E-mail address: a.harrison@imperial.ac.uk (A.C. Twitchett-Harrison).
[1] Now at: Center for Electron Nanoscopy, Technical University of Denmark, DK-2800 Kongens Lyngby, Denmark.

0304-3991/$ - see front matter © 2008 Elsevier B.V. All rights reserved.
doi:10.1016/j.ultramic.2008.05.014

Under these conditions, the measured phase shift is a monotonic, linear function of the specimen thickness, and therefore satisfies the projection requirement for electron tomography.

Off-axis electron holography has been successfully used to characterise semiconductor device structures in 2D [1,2], but the limiting factor for the quantification of experimental results has been the impact of specimen preparation and the presence of surface potentials on the variation in electrostatic potential as a function of depth into the thin specimen. For examination using off-axis electron holography, a thin, parallel-sided membrane should be prepared containing the area of interest adjacent to an area of vacuum. Focused ion beam (FIB) milling is currently the most promising specimen preparation method that can offer the site-selection required for the preparation of device structures. However, the ion milling leaves thick layers with modified physical and electrical properties at the surfaces of the specimen. Recent work has investigated the reduction of the thickness of these layers through the use of lower-energy ion beams [8], and has reduced the thickness of the amorphous surface layer. However, it is the electrical properties that are critical to the performance of the device structure, and therefore these must be characterised carefully when measuring the electrostatic potential distribution. Electron holography experiments have been carried out using specialist TEM holders that allow an electrical bias to be applied to the device specimen *in-situ* in the electron microscope. This ensures that the device is examined under conditions that are as close to working conditions as possible [9], essential for obtaining an accurate characterisation of the electrostatic properties of the device structure.

Previous work has reported briefly on the 3D potential distribution in a silicon semiconductor device structure, revealing the expected variation in potential arising from a combination of the presence of surfaces and ion beam damage [5]. In this paper, we elucidate further the experimental details for the acquisition and reconstruction of holographic tomograms for the characterisation of 3D electrostatic potential distributions.

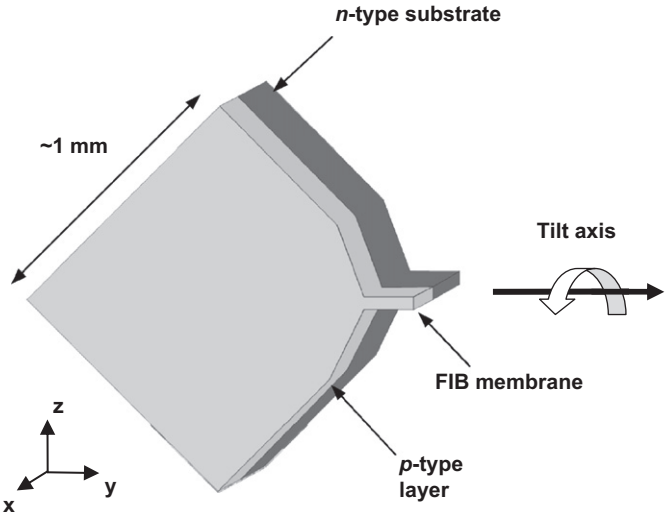

Fig. 1. Schematic diagram illustrating the geometry of the FIB-prepared p–n junction for combined electrical biasing, tomography and holography experiments in the TEM.

2. Experimental details

A silicon p–n junction device comprising a 2.5 μm-thick p-type (B-doped) layer on an n-type (Sb-doped) substrate was prepared for examination in the TEM using 30 kV FIB milling in a novel specimen geometry, illustrated in Fig. 1. This geometry allows a parallel-sided specimen to be prepared in a site-specific location, which can be tilted to high angles in the electron microscope without obscuring any of the thin area. Two specimens of different thickness were prepared. The crystalline thicknesses were determined using convergent beam electron diffraction (CBED) to be 330 ± 15 and 480 ± 15 nm. Taking the electrically inactive crystalline layer to be 25 nm thick at each surface (measured from the same specimens) [10], the specimen thicknesses in the tomographic reconstructions were constrained to be 280 and 430 nm for the thin and thick specimens, respectively. By comparison with the t/λ measurements obtained from reconstructed holographic amplitude images [11] (where λ is the inelastic mean-free path), the measured values of λ are 135 ± 20 and 115 ± 20 nm, respectively. The specimens were mounted in a cartridge-based custom-built electrical biasing holder [12], which allows two electrical connections to be made to the specimen *in-situ* in the electron microscope for examination and characterisation of an electrically biased device. Off-axis electron holography was performed on a Philips CM300 FEGTEM operated at 200 kV equipped with electrostatic biprism and a 'Lorentz' objective mini-lens. A biprism voltage of between 70 and 100 V was used to obtain fringe spacings of between 6.6 and 5.1 nm with an overlap width of 700–860 nm. Conditions were kept constant throughout each tilt series, but were optimised for each specimen. Typical levels of fringe contrast were 20% in the vacuum region, with a minimum fringe contrast of 6% in the specimen. The thinner p–n junction specimen was examined under an applied electrical reverse bias of 0, 2, and 3 V, and the thicker specimen was examined under applied electrical reverse bias of 0 and 2 V. Holograms were acquired digitally using a 2048×2048 pixel charge-coupled device (CCD) camera with a reference (empty) hologram acquired for every object hologram. A series of holograms was acquired for each specimen under each biased condition with specimen tilt angles from -66° to $+60^\circ$ with a tilt increment of 2°.

3. Holographic data processing

Phase and amplitude images were reconstructed using the process illustrated schematically in Fig. 2(a–e) from the electron holograms using the image processing programme SEMPER [13]. To optimise the phase resolution, the mask placed around the sideband was reduced in size from the maximum value [14] to give a spatial resolution of 25 nm and a phase resolution of 0.1 rad in the reconstructed phase images [15]. The phase images were unwrapped to remove the phase wraps that arise from gradual phase variations across the specimen. However, the stacking of phase wraps at the abrupt specimen edge could not be unwrapped because the phase gradient was too steep, thereby giving rise to many phase wraps within only a few pixels, as illustrated in Fig. 3. The phase values within the p- and n-type regions of the specimen in the as-reconstructed phase images were, therefore, shifted by an unknown number of phase wraps relative to the vacuum level, and must be adjusted to create a consistent data set before the phase data can be used for tomographic reconstruction. This can be achieved by setting the average phase value across the p–n junction to a fixed (nominal) value, an approach which is suitable for reconstructing the relative phase variation around the p–n junction. This approach is only valid if reconstructing (tomographically) a sub-region of the phase image that is contained entirely within the specimen, therefore excluding any vacuum regions (as illustrated by the marked box in Fig. 2(g)). If, however, the mean inner potential of the specimen is of interest, then the number of phase wraps can be calculated by using the

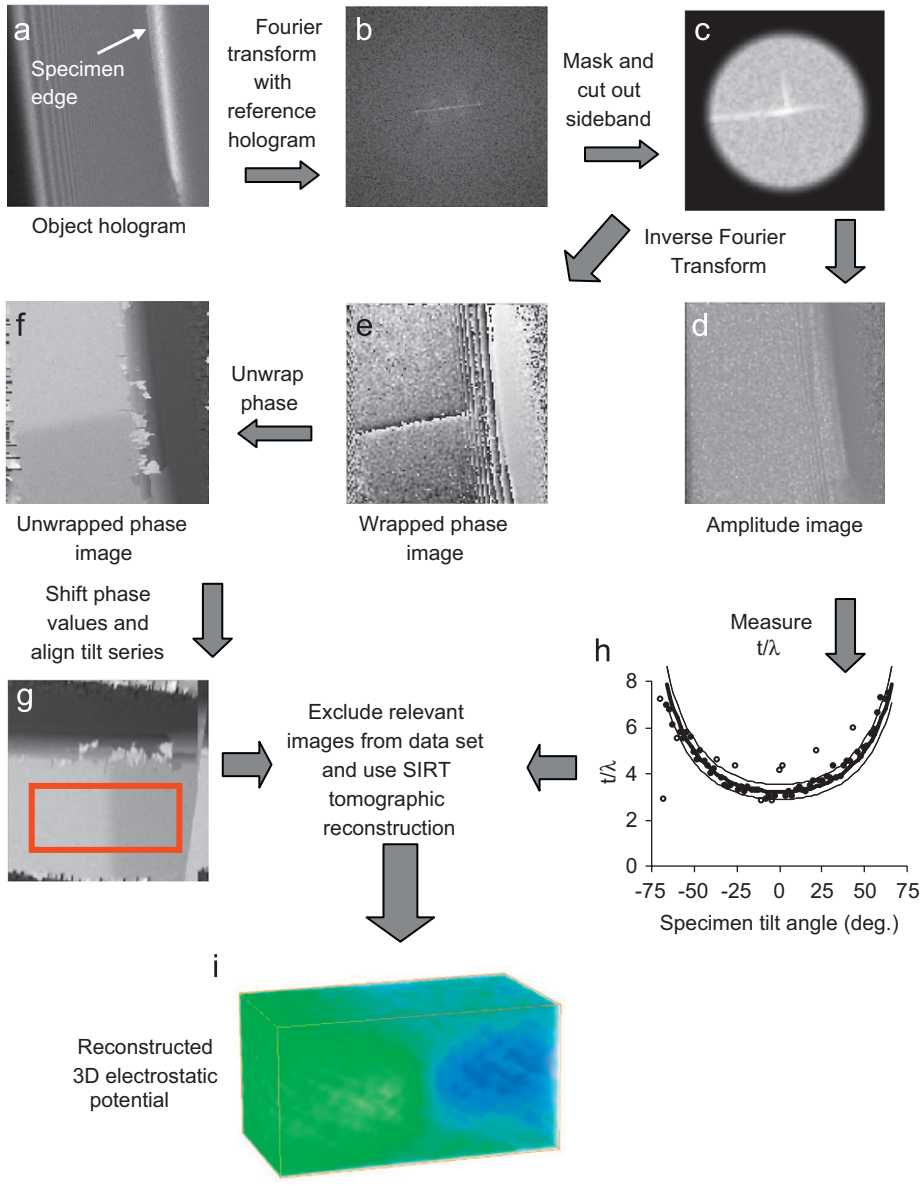

Fig. 2. Schematic diagram representing the holographic reconstruction process (steps (a–e)) and subsequent data processing required for tomographic reconstruction of the 3D electrostatic potential (steps (f–i)).

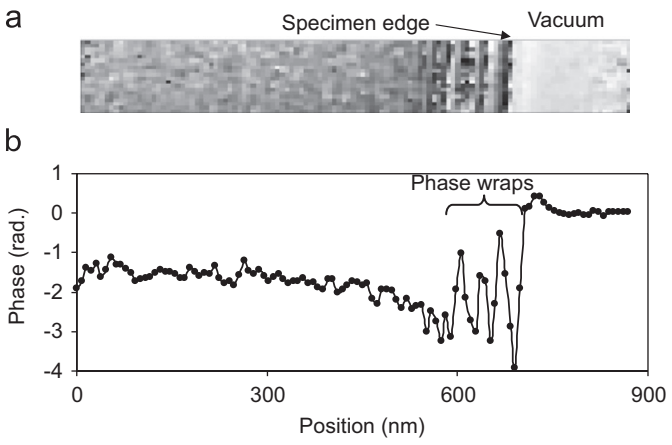

Fig. 3. (a) Extracted region from an experimental wrapped phase image with the projected phase profile (b) from the extracted region illustrating the presence of noise and multiple phase wraps at the specimen edge.

thickness measurements (from t/λ) to determine the expected phase shift, and thereby estimate how many integer multiples of 2π must be added to the phase images to recover the correct phase level within the specimen. For this work, the *relative* phase variation was reconstructed, and therefore the average phase shift measured across the p–n junction was set to a value of zero. This process of reconstruction and data adjustment was performed for each phase image within the tilt series of holograms.

To optimise the results obtained using off-axis electron holography, all contributions to the observed phase shift in the electron wave other than the contribution of interest should be minimised. If thickness variations are present across the area of interest, then the mean inner potential contribution to the phase shift observed in a 2D phase image can be much greater than the dopant-related potential contribution, masking the information of interest. The specimens examined in this study were parallel-sided and, therefore, no thickness-related mean inner potential variations were observed across the area of interest. Marker particles for tomographic alignment purposes may affect the

charge distribution in the specimen and introduce artefacts by obscuring the signal of interest, and therefore were not used in this investigation. Alignment of the tilt series of reconstructed holographic phase images was performed by measuring the position of the edge of the specimen in the original hologram (as shown in Fig. 2(a)), and this information was then used to rotate the respective reconstructed phase image to align the edge in the *y*-direction. The position of the p–n junction was then used to align the rotated reconstructed phase images in the *x*-direction. Fig. 2(g) shows an aligned reconstructed 2D phase image.

During a tomographic tilt series, a crystalline specimen will pass through many strongly diffracting conditions. When the specimen is in a strongly diffracting condition, the projected potential is not a monotonic function of the specimen thickness, and therefore does not satisfy the projection requirement. The holograms acquired under such conditions must, therefore, be identified and excluded from the tomographic reconstruction. The affected images can be identified using the t/λ maps that can be calculated from the amplitude image reconstructed from off-axis electron holograms. Fig. 2(h) shows a plot of t/λ measured at the p–n junction position as a function of tilt angle. This should reflect the variation in thickness as a function of specimen tilt, and the data should, therefore, follow a $t_0/\lambda\cos(\theta)$ variation (where t_0 is the thickness at zero degrees tilt and θ is the tilt angle) as indicated by the bold solid line. The data points that lie away from the expected variation (as indicated by open data points) indicate specimen tilt angles where strong diffraction contrast is present, and therefore the phase images acquired at these specimen tilt angles must be excluded from the tomographic reconstruction. The dotted lines represent 10% above and below the expected t/λ value, and are used to provide boundaries beyond which the data points are deemed to lie outside the expected range, allowing for experimental error.

4. Tomographic data reconstruction

Tomographic reconstruction was performed using INSPECT3D software [16]. Although this programme is routinely used for the alignment of a tilt series of images, for the holographic data the standard alignment routines are unsuccessful due to the lack of fine features and high-frequency information in the images. Many of the features in a phase image are artefacts, including the Fresnel fringes from the edge of the biprism and the phase wraps present at the specimen–vacuum interface. The phase features of interest are potential variations that are continuous in nature, in contrast to the isosurfaces that are usually of interest in tomographic reconstruction, and therefore considerable care must be taken when using any standard tomographic alignment or reconstruction process. A number of tomographic reconstruction methods are routinely used; these include back projection and iterative methods [7,16]. Weighted back projection methods apply a filter to the data to remove low-frequency information and enhance the high-frequency data. However, for holographic tomography, it is the medium to low-frequency information present within the phase images that is of interest, and therefore an alternative technique must be used. The simultaneous iterative reconstruction technique (SIRT) is a method that iterates and minimises the differences between the reconstructed tomogram and the original data during reconstruction [17]. If too many iterations are performed, this reconstruction algorithm enhances unwanted noise, and too few iterations reduce the phase gradient across the p–n junction, as illustrated in Fig. 4. The optimal number of iterations was found to be approximately 15.

A limited maximum tilt angle of the experimental data set results in the elongation of the tomographic reconstruction in the *z*-direction due to the 'missing wedge' of information [18]. However, by constraining the thickness in the SIRT tomographic reconstruction using independent specimen thickness measurements, some of this missing information is provided. Following Eq. (1), to extract quantitative information from the reconstructed phase volume, it is crucial to know the thickness over which a measured phase shift has occurred. It is particularly important to be able to establish an independent, accurate measurement of the specimen thickness to be able to constrain the tomographic reconstruction to the correct thickness. Although t/λ plots can be used to estimate the specimen thickness, λ is in general not well defined and is dependent on the electron optical conditions, in addition to being strongly specimen dependent. As a relative thickness measurement, t/λ can be invaluable, but it should not be relied upon for absolute thickness determination. For this study, the specimen thickness was measured using CBED to quantify the crystallographic thickness of the membranes. Previous results have revealed that, for Si specimens prepared using 30 kV Ga ion

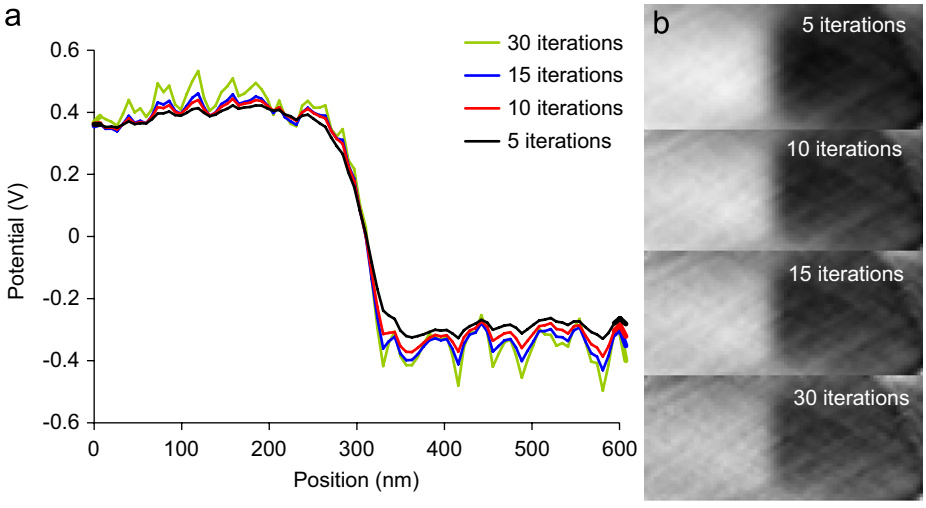

Fig. 4. (a) Line traces extracted from the centres of tomographic reconstructions of the 330 nm-thick specimen. The tomographic reconstructions were performed using different numbers of iterations in the SIRT algorithm. Above 15 iterations, the noise level is enhanced and reduces the quality of the tomographic reconstruction of the relatively low-frequency electrostatic potential and (b) 2D projections of the tomographic reconstructions illustrating the change in the noise levels as a function of number of iterations.

milling, a 25 nm-thick crystalline, electrically inactive layer is present near each specimen surface [10]. This allowed the electrically active specimen thickness to be calculated from the CBED results for these specimens.

The tilt axis cannot be aligned accurately for tomographic reconstruction of the phase images, because the lack of fine features in the specimen results in reconstructed slices (that are usually used to adjust the position of the tilt axis) that are relatively insensitive to the exact position and orientation of the tilt axis. However, it is known that the tilt axis passes through the point to which all of the images were aligned. The errors arising from the misalignment of the tilt axis were experimentally examined, and the tomographic reconstructions were found to be relatively insensitive to the angle and position of the tilt axis (to within $<10^\circ$ rotation and <10 pixels) [19].

To obtain a quantitative interpretation of the data, projections of the reconstructed tomograms were compared to the original phase images. A 'scaling' factor between the tomographic data and original phase images was determined, thus allowing the 'intensity' values in the individual voxels in the tomograms to be converted to the phase shift that would be observed as the electron beam passes through a thickness of material equal to the *z*-dimension of each voxel. Ultimately, the 3D electrostatic potential distribution can be calculated from the 3D phase shifts.

5. Experimental results and discussion

Experimental holograms acquired from the p–n junction specimen under applied bias conditions of 0, 2, and 3 V were reconstructed. The phase shift within the specimen was normalised to the mean value between p- and n-type to reconstruct a tomogram of the *relative* electrostatic potential and not the mean inner potential. The thicknesses of the tomographic reconstructions were constrained to the electrically active thicknesses of the membranes, 280 and 430 nm.

The experimental data sets for the thinner specimen each contained 63 images. Between 18 and 23 images were excluded from each data set before tomographic reconstruction. Experimental data sets acquired using the thicker specimen at 0 and 2 V reverse electrical bias contained 51 images, from -50° to $+50^\circ$. Holograms acquired at specimen tilt angles of greater than 50° were limited by signal-to-noise (at 50° tilt, the total effective specimen thickness is >810 nm), which was insufficient to reconstruct the phase information within the specimen.

Fig. 5(a) and (b) shows tomographic reconstructions of the 0 V data sets for both specimens. The data have been reconstructed using INSPECT3D using the SIRT algorithm with 15 iterations. The thickness was constrained in the tomographic reconstruction to the electrically active specimen thickness (to within the nearest voxel). The voxel size is 12.8 nm, and the spatial resolution is approximately 25 nm in the *x*–*y* plane and 40 nm in the *z*-direction, with a corresponding electrostatic potential resolution of ~0.2 V. These values for resolution are estimates as an accurate determination of the spatial resolution is difficult to calculate. Many standard methods for calculating the spatial and signal resolution (see Ref. [7] for examples) rely on a discrete object of interest. With the extended object of interest in this study, these methods do not produce meaningful results and therefore could not be applied.

Fig. 5(c) shows line traces from the tomographic reconstructions revealing the electrostatic potential as a function of position within the specimen. These data allow the surface effects to be separated from the properties of the material found in the centre of the specimen by extracting information from voxels at defined distances from the membrane surface. The line traces can be used to assess the depletion width and built-in potential of the p–n junction as a function of position within the specimen. The 'top'

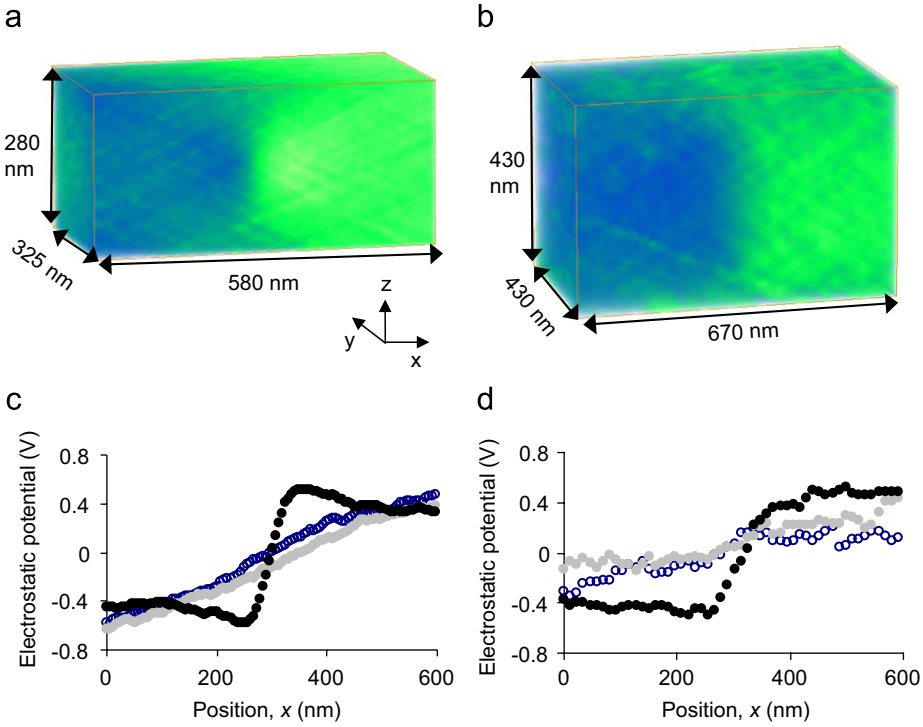

Fig. 5. Tomographic reconstructions of the (a) 330 nm-thick and (b) 480 nm-thick (crystalline thickness) specimens under 0 V applied electrical bias. Plots of the electrostatic potential variation as a function of *x* at the top (open circles), centre (black data points) and bottom (grey data points) for the (c) 330 nm- and (d) 480 nm-thick specimens. The slow variation in the electrostatic potential at the surfaces of the tomographic reconstructions is characteristic of a significant reduction in the electrically active dopant concentrations compared to the electrically active dopant concentration in the centre of the specimens.

and 'bottom' traces extracted from the tomographic reconstructions adjacent to the electrically inactive (but crystalline) near-surface layers reveal very slowly varying electrostatic potential across the junction position. However, the line traces extracted from the centre of the specimen show a sharply varying electrostatic potential distribution that is characteristic of a p–n junction in a bulk semiconductor. The built-in potential is not highly sensitive to the electrically active dopant concentration; however, the width of the charge separation region does show a more marked dependence on the electrical activity of the semiconductor junction. The wide charge depleted regions observed at the surfaces of the reconstructed volumes reveal a significant reduction in the electrically active dopant distribution compared to that present in the centre of the specimen. This reduction in the electrically active dopant concentration in the near-surface regions is likely to arise from a combination of effects. Specimen preparation using FIB milling is known to create damage that alters the electrical properties of the semiconductor [10]. In addition, the presence of surfaces in semiconductors can change the electrostatic potential distribution within a thin specimen significantly [20].

To investigate the variation in electrostatic properties as a function of depth into the specimen, line traces were extracted at every voxel as a function of z-position. The dependence of the depletion width on z-position was only observed in the vicinity of the surfaces of the tomogram. Close to the centre of the tomogram, a thickness was measured across which the p–n junction depletion width was approximately constant (within experimental error). This thickness was measured to be 35 nm for the 330 nm-thick specimen and 190 nm for the 480 nm-thick specimen. Although these data only provide two measurements to which to fit a trend, they indicate that within the electrically active specimen thickness there are 125 ± 40 nm-thick layers at each surface of the tomogram in which the electrical activity of the specimen is varying, and does not represent bulk-like properties. It is encouraging to note that the electrical properties do reach a region of invariance indicating that 'bulk-like' properties are reached in the centre of the membrane, where the measured properties are the same (within experimental error) from the thin and the thick specimen. The depletion width in this region is measured to be 110 ± 25 nm for the thin specimen and 115 ± 25 nm for the thick specimen, corresponding to electrically active dopant concentrations of $\sim 2 \times 10^{17} \pm 2 \times 10^{17}$ cm^{-3} for both specimens.

Further quantification of the electrostatic potential can be obtained through the fitting of the line traces. The fitted profiles can subsequently be differentiated to reveal the electric field and charge density distribution within the specimen. Fig. 6 shows both experimental and fitted profiles for the 330 nm-thick specimen under 2 V reverse bias, with the associated electric field distribution (calculated via Poisson's equation). Further details about the quantitative results extracted from these data sets can be found in [5]. To improve the quantification of the electric field and charge distribution, the spatial resolution must be optimised, and in this study, the spatial resolution of the reconstructions was limited to improve the phase resolution. Recent studies have indicated that [21], with improvements in microscope technology, longer acquisition times can be used to achieve higher spatial and phase resolutions. This combined technique has significant promise to be able to map electrostatic potential distributions with sub-10 nm spatial resolution and sub-0.1 V potential sensitivity.

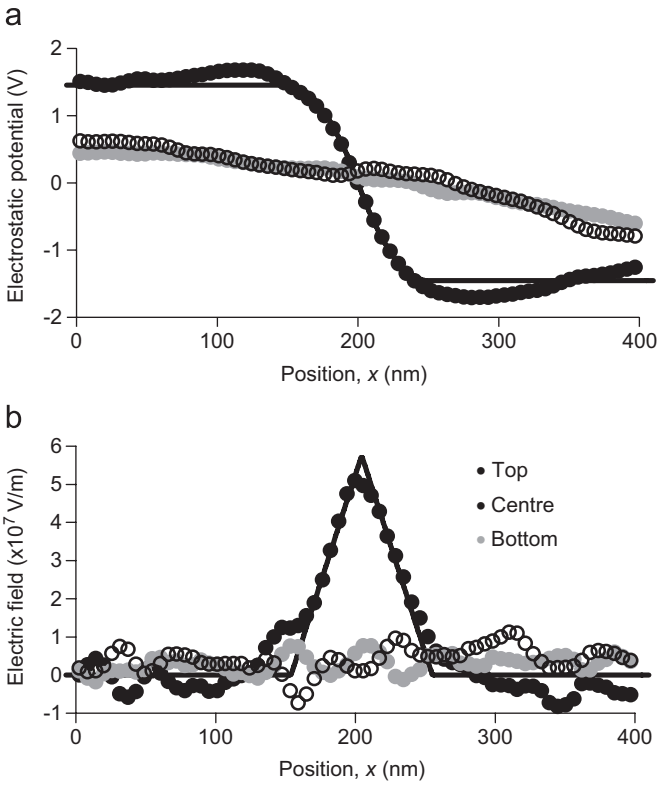

Fig. 6. Plots of the (a) electrostatic potential and (b) electric field variation as a function of distance across the p–n junction extracted at the top, centre and bottom of the tomographic reconstruction for the 330 nm-thick sample under 2 V applied electrical reverse bias.

6. Conclusions

These results indicate that the technique of tomographic holography can be used to measure the quantitative, 3D electrostatic potential distributions in both unbiased and electrically biased semiconductor device structures. Whilst electron tomography has been successfully applied to a number of biological and materials science problems over recent years, the application of electron holography in combination with electron tomography provides an exciting new method for the examination of electrostatic potentials in three dimensions with nanometre resolution. This paper has described some of the aspects of the development of this combined technique for its application to simple semiconductor device structures and has highlighted the quantitative nature of the experimental results. However, future development of this technique is required to improve the tomographic reconstruction algorithms and experimental data acquisition, which will result in reduced reconstruction artefacts and improved spatial and phase resolution. The application of additional constraints, for example, known boundary conditions, and the use of a higher specimen tilt range with specimens of different geometry, for example, nanowires or finger-shaped specimens, will improve the quality of the data reconstructions. Additionally, incorporating methods that iterate between experimental data and simulated electrostatic potential during tomographic reconstruction would lead to improved interpretation of the 3D potential distribution.

Acknowledgements

The authors would like to thank Philips Research (Eindhoven) for providing the specimen and Simon Newcomb (Glebe Scientific, Ireland) for assistance with specimen preparation.

References

[1] M.A. Gribelyuk, M.R. McCartney, J. Li, C.S. Murthy, P. Ronsheim, B. Doris, J.S. McMurray, S. Hedge, D.J. Smith, Phys. Rev. Lett. 89 (2002) 025502.
[2] W.D. Rau, P. Schwander, F.H. Baumann, W. Höppner, A. Ourmazd, Phys. Rev. Lett. 82 (1999) 2614.
[3] N. Duhayon, et al., J. Vac. Sci. Technol. B 22 (1) (2004) 385.
[4] www.itrs.net.
[5] A.C. Twitchett-Harrison, T.J.V. Yates, S.B. Newcomb, R.E. Dunin-Borkowski, P.A. Midgley, Nano Lett. 7 (7) (2007) 2020.
[6] P.A. Midgley, M. Weyland, Ultramicroscopy 96 (3–4) (2003) 413.
[7] J. Frank (Ed.), Electron Tomography: Three-Dimensional Imaging with the Transmission Electron Microscope, Plenum Press, New York, London, 1992.
[8] D. Cooper, R. Truche, J.-L. Rouviere, Ultramicroscopy 108 (5) (2008) 488.
[9] A.C. Twitchett, R.E. Dunin-Borkowski, R.J. Hallifax, R.F. Broom, P.A. Midgley, Microsc. Microanal. 11 (2005) 1.
[10] A.C. Twitchett, R.E. Dunin-Borkowski, P.A. Midgley, Phys. Rev. Lett. 88 (23) (2002) 8302.
[11] M.R. McCartney, M. Gajdardziska-Josifovska, Ultramicroscopy 53 (3) (1994) 283.
[12] R.E. Dunin-Borkowski, A.C. Twitchett, J.S. Barnard, R.F. Broom, P.A. Midgley, A.C. Robins, D.W. Smith, J.J. Gronsky, P.E. Fischione, Microsc. Microanal. 10 (Suppl. 2) (2004) 1012.
[13] W.O. Saxton, T.J. Pitt, M. Horner, Ultramicroscopy 4 (3) (1979) 343.
[14] G. Ade, Electron holography, In: A. Tonomura, L.F. Allard, G. Pozzi, D.C. Joy, Y. Ono (Ed.), Elsevier Science B. V., 1995, p. 33
[15] H. Lichte, Ultramicroscopy 38 (1991) 13.
[16] www.fei.com.
[17] P. Gilbert, J. Theor. Biol. 36 (1972) 105.
[18] R.A. Crowther, D.J. De Rosier, A. Klug, Proc. R. Soc. London A 317 (1530) (1970) 319.
[19] T.J.V. Yates, The Development of Electron Tomography for Nanoscale Materials Science Applications, University of Cambridge, Cambridge, UK, 2005 Ph.D. Thesis.
[20] R.E. Dunin-Borkowski, W.O. Saxton, Acta Crystallogr. A 53 (1997) 242.
[21] D. Cooper, R. Truche, P. Rivallin, J.-M. Hartmann, F. Laugier, F. Bertin, A. Chabli, J.-L. Rouviere, Appl. Phys. Lett. 91 (2007) 143501.